Title: Vasomotion as a driving force for paravascular clearance in the awake mouse brain

Susanne J. van Veluw PhD, Steven S. Hou PhD, Maria Calvo-Rodriguez PhD, Michal Arbel-Ornath PhD, Austin C. Snyder BS, Matthew P. Frosch MD PhD, Steven M. Greenberg MD PhD, Brian J. Bacskai PhD

Supplemental Figures: 7

Supplemental Figures

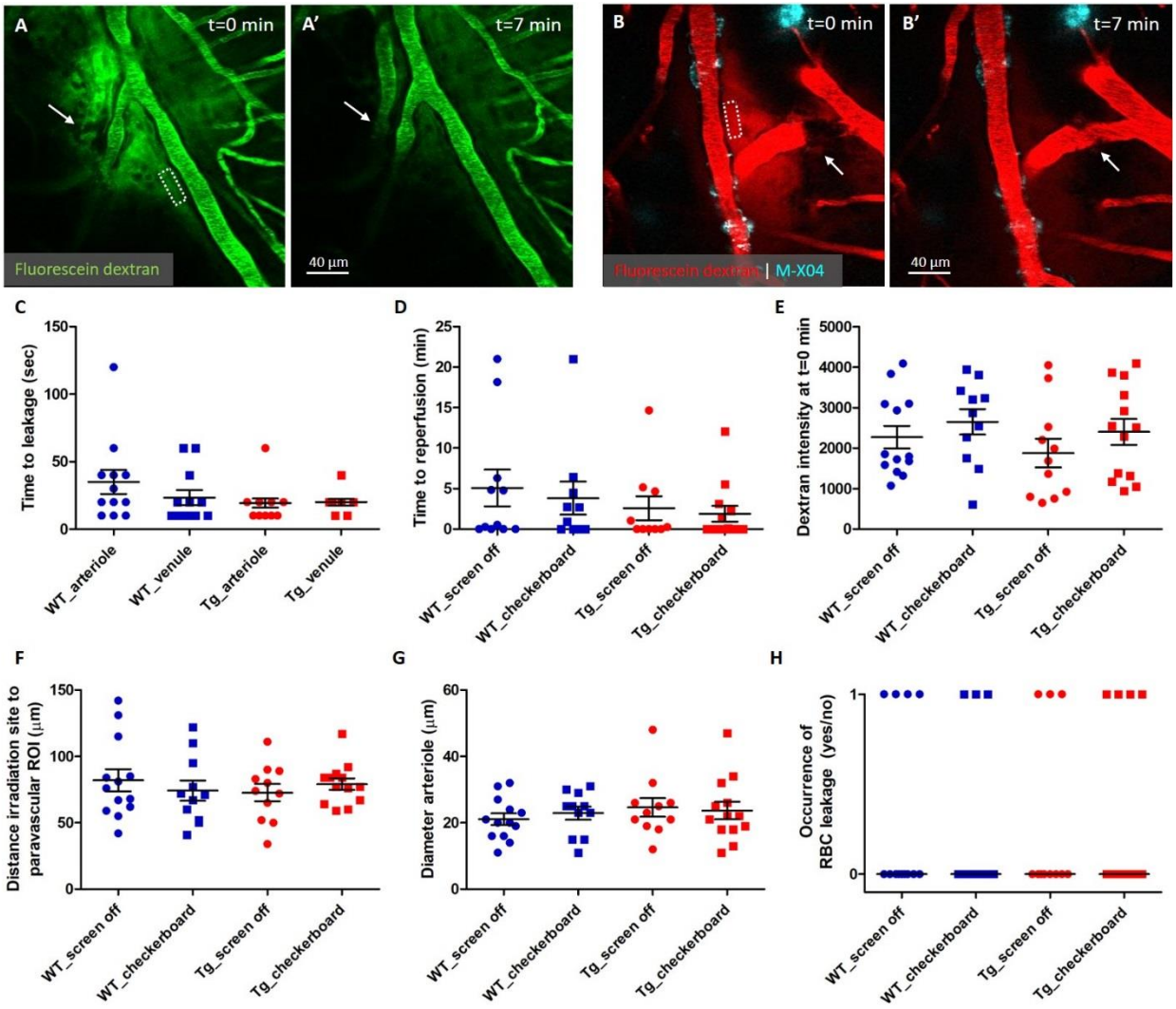

Supplemental Figure 1 (related to Figure 3). Vessel irradiation is methodologically comparable between wild-type and transgenic mice.

To measure clearance rates alongside arterioles, neighboring venules or arterioles were irradiated to allow fluorescein dextran to extravasate into the parenchyma (AB). Note: fluorescein dextran is depicted in red for better contrast with Aβ in cyan (B). Vessel irradiation was immediately stopped when dextran was observed to leak out of the vessel. Time to leakage was comparable between wild-type (WT) and transgenic (Tg) mice and vessel type (C; WT: on average 35 seconds for arterioles and 23 seconds for

venules, Tg: on average 21 seconds for arterioles and 20 seconds for venules). Time to restored flow in the irradiated vessel (*i.e.* time to reperfusion) was determined based on the recorded time-course after vessel irradiation and was also found to be comparable between mice and conditions (D; WT: on average 5.1 minutes during screen off and 3.8 minutes during visual stimulation, Tg: on average 2.6 minutes during screen off and 1.9 minutes during visual stimulation). Note: excluding measurements resulting from the 5 vessels with time to reperfusion >10 min did not notably alter the reported findings in clearance rates between WT and Tg mice. Panel AB and A'B' are representative images to illustrate clot formation and co-occurring vessel blockage immediately after vessel irradiation (AB; arrow) and restoration of flow within minutes (A'B'; arrow) in a WT (AA') and a Tg mouse (BB'). The amount of extravasated dextran, quantified as dextran intensity at t=0 minutes within the paravascular ROI (dashed ROIs in A and B), was also comparable between mice and conditions (E; WT: on average 2268 for screen off and 2649 for visual stimulation measurements, Tg: on average 1878 for screen off and 2401 for visual stimulation measurements). The distance between irradiation site and paravascular ROI was comparable between mice and conditions (F; WT: on average 82 µm for screen off and 74 µm for visual stimulation measurements, Tg: on average 73 µm for screen off and 79 µm for visual stimulation measurements), as was the diameter of the arteriole alongside which clearance was measured (G; WT: on average 21 µm for screen off and 23 µm for visual stimulation measurements, Tg: on average 25 µm for screen off and 24 µm for visual stimulation measurements). Finally, the occurrence of small numbers of red blood cell (RBC) leakage after vessel irradiation was also comparable between mice and conditions (H; 0=no, 1=yes, median for all groups is 0). Error bars in C-G represent standard error of the mean.

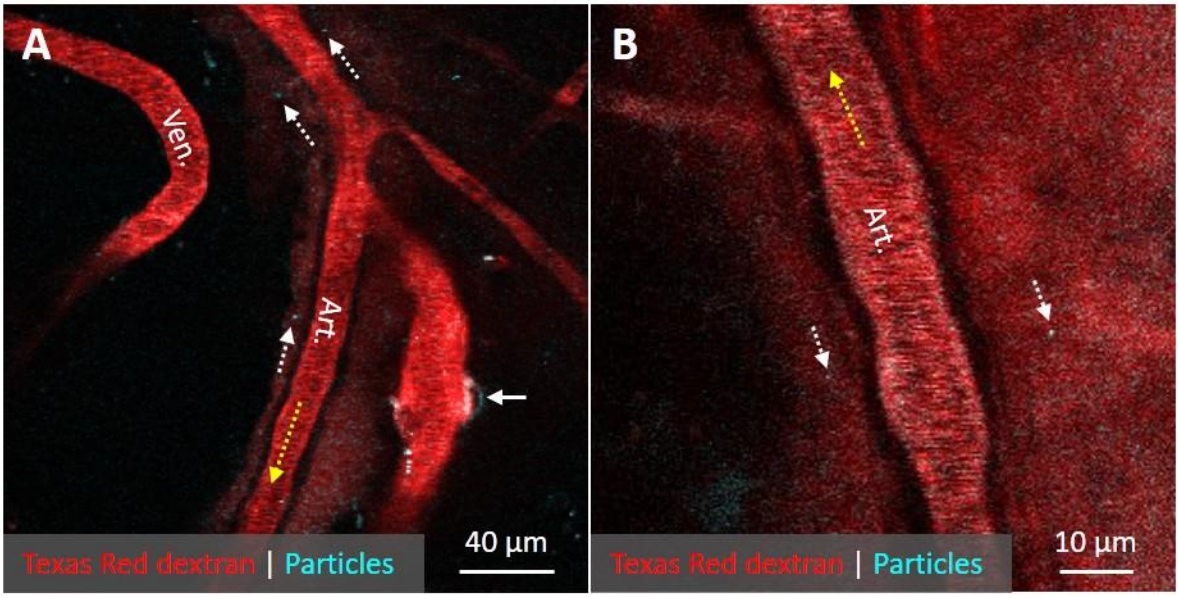

Supplemental Figure 2 (related to Figure 3). Both fluorescent dextran and nanoparticles line up alongside arterioles after focal vessel irradiation and individual particles can be observed to clear in the opposite direction of blood flow in awake head-fixed wild-type mice.

To provide an independent way to demonstrate paravascular clearance, blue fluorescent nanoparticles were co-injected with 70 kDa Texas Red dextran prior to imaging in n=3 C57BL/6J mice with chronic cranial windows over the right visual cortex. A 5-minute recording at 2x magnification immediately after focal vessel irradiation in a nearby arteriolar branch (A; arrow points at the irradiation site) reveals dissipation of dextran and nanoparticles alongside the arteriole, but not the venule (A). Particles were observed moving in the opposite direction of blood flow (yellow broken arrow indicates direction of blood flow and white broken arrows indicate direction of individual particles). Higher frame-rate 30-second recordings at 6x magnification in a different mouse confirmed these observations of slow-moving particles immediately adjacent to the arteriole in opposite direction of blood flow (B; yellow broken arrow indicates direction of blood flow and white broken arrow indicates direction of individual particles). See also Supplemental Video 2. Note: brightness and contrast were adjusted for panel A and B.

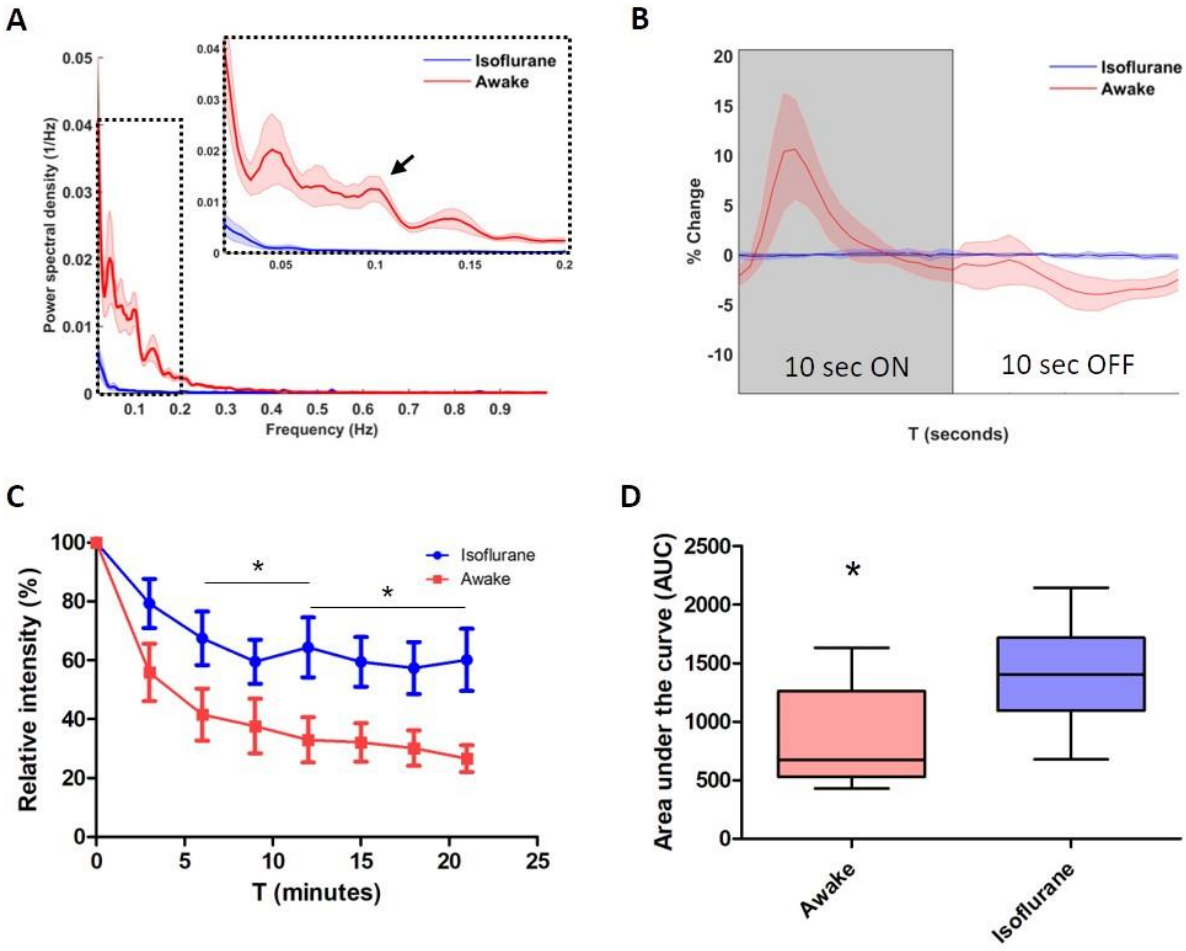

Supplemental Figure 3 (related to Figure 3). Deep isoflurane anesthesia reduces vasomotion and evoked vascular reactivity as well as paravascular clearance rates compared to the awake state.

To assess the effect of reduced vasomotion on clearance rates, n=4 C57BL/6J mice with chronic cranial windows over the right visual cortex were imaged under deep isoflurane (2.5%) anesthesia and awake. Vasomotion was observed to be significantly reduced during isoflurane imaging compared to awake (A), as well as the response to visual stimulation (B). Likewise, clearance rates under isoflurane anesthesia were significantly reduced, as quantified by lower relative dextran intensities at t=12 minutes (C; 64 ± 29 % under isoflurane (n=8 vessels) vs. 33 ± 23 % awake (n=9 vessels), t-test, p=0.024) and t=18 minutes (C; 57 ± 25 % under isoflurane vs. 30 ± 18 % awake, t-test, p=0.020) and AUC (D; 1403 ± 453 under isoflurane vs. 881 ± 427 awake, t-test, p=0.027). Shaded areas in A represent standard error of the mean, and in B

standard deviations. Error bars in C represent standard error of the mean. Median and range are indicated in D. * $p<0.05$.

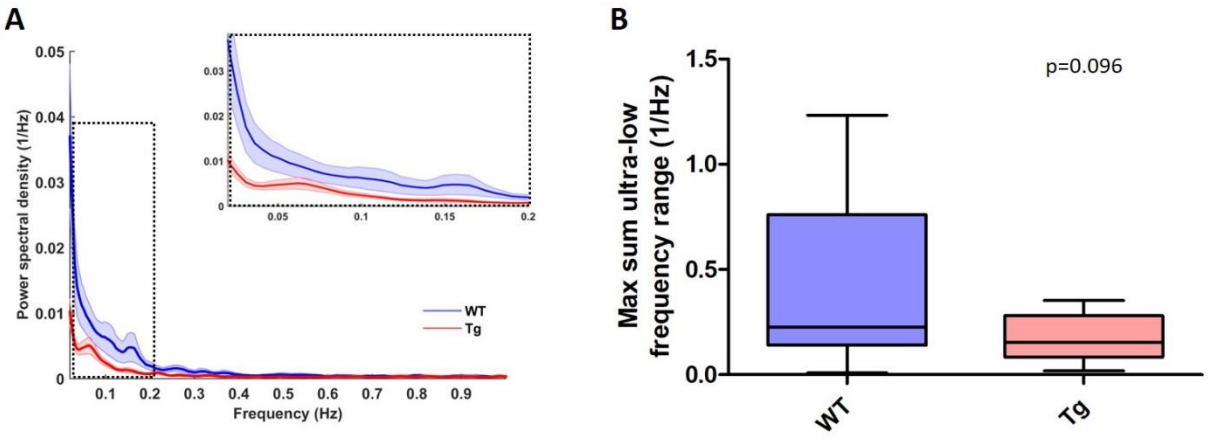

Supplemental Figure 4 (related to Figure 4). Spontaneous vasomotion (around 0.1 Hz) is reduced in 14 months old APP/PS1 mice.

A sub-set of APP/PS1 transgenic (Tg) and wild-type (WT) mice were imaged again on average ~4-5 months later around 14 months old to assess the effect of aging and increased cerebral amyloid angiopathy burden on spontaneous vasomotion. Spontaneous arteriolar oscillations were recorded over a 5-minute time course at 2x magnification, a resolution of 128x128, and frame rate of ~5.3 Hz. At this age the averaged Fourier plot revealed reduced vasomotion in both groups, and no prominent peaks centered around 0.1 Hz (A). The maximum sum of the power in the ultra-low frequency range (<0.4 Hz) was lower in Tg mice (0.16 ± 0.10 1/Hz, n=11 vessels in 8 mice) compared to WT mice (0.38 ± 0.38 1/Hz, n=11 vessels in 8 mice, t-test, p=0.096) (B). Shaded areas in A represent standard error of the mean. Median and range are indicated in B.

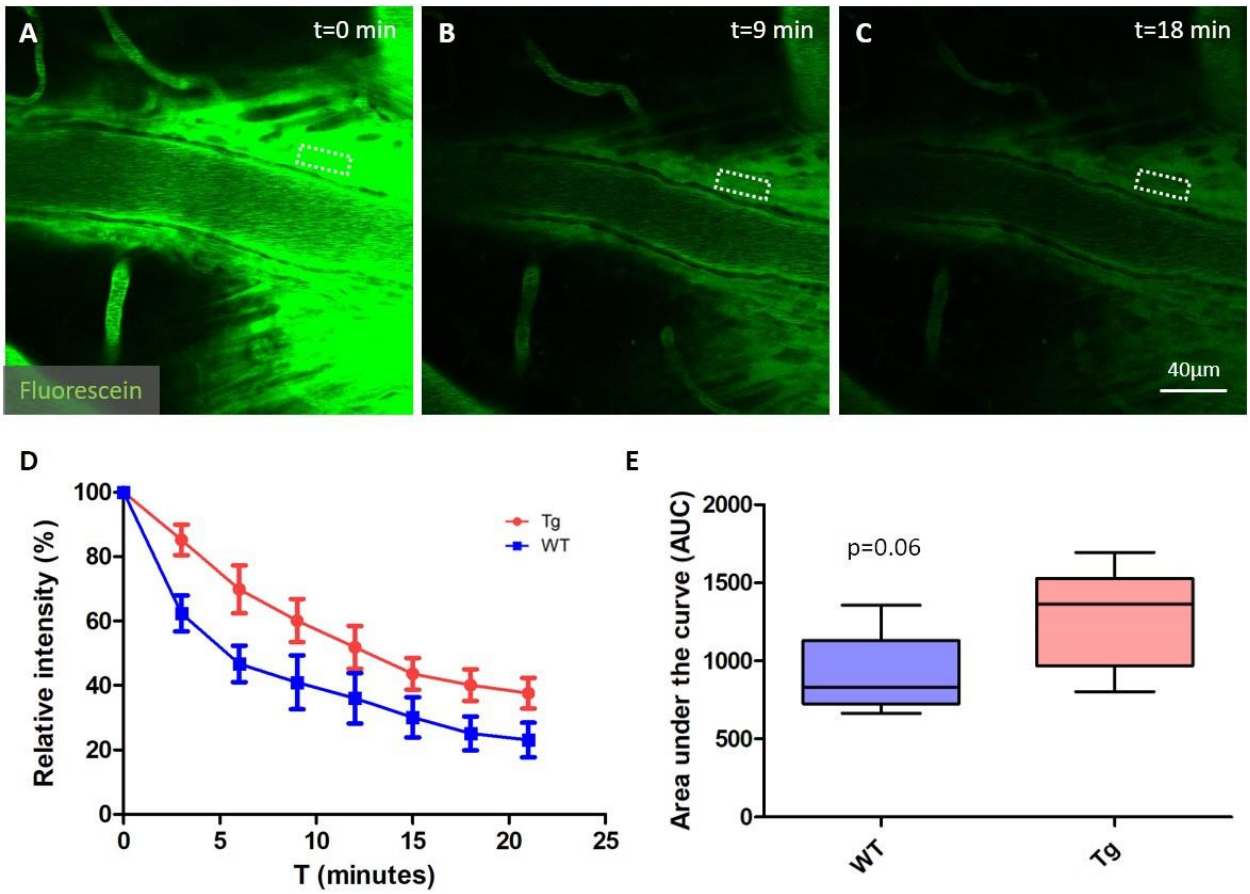

Supplemental Figure 5 (related to Figure 5). Paravascular clearance rates of unconjugated fluorescein are reduced during visual stimulation in 8-10 months old APP/PS1 mice.

Intravenously injected unconjugated fluorescein is rapidly cleared from the circulation and extravasates from arterioles (ABC). Quantification of the fluorescein decay curves on maximum intensity projections revealed slower clearance rates during visual stimulation in transgenic (Tg) compared to wild-type (WT) mice (D), as expressed by area under the curve (AUC) (E; 1259 ± 319 in Tg vs. 909 ± 265 in WT, t-test, p=0.060). Median and range are indicated in E.

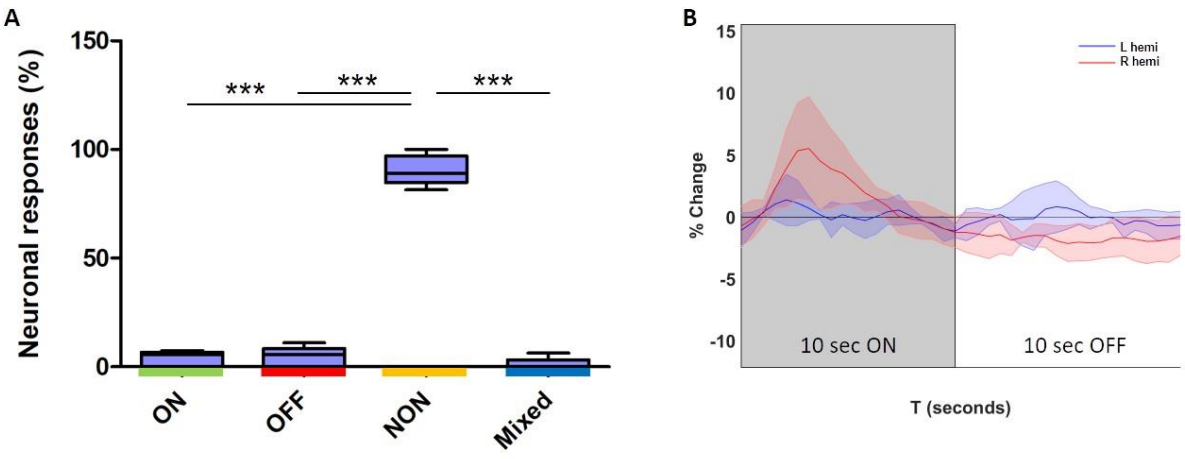

Supplemental Figure 6 (related to Figure 6). Responses to visual stimulation are largely restricted to the visual cortex.

Neuronal responses to visual stimulation were recorded in the bilateral somatosensory cortex in n=2 awake C57BL/6J mice. Only 4% (out of a total number of 100) neurons met the criteria to be classified as an ON-responder, whereas 90% of neurons were NON-responders (A; t-test, $p<0.0001$). Interestingly, a small hemodynamic response was observed in the arterioles in the ipsilateral hemisphere (*i.e.* the right hemisphere), but no responses in the contralateral hemisphere (*i.e.* the left hemisphere) (n=8 arterioles in total in 2 mice) (B), which suggests that the responses are largely restricted to the visual cortex. Median and range are indicated in A. Shaded areas in panel B represent standard deviations. *** $p<0.001$.

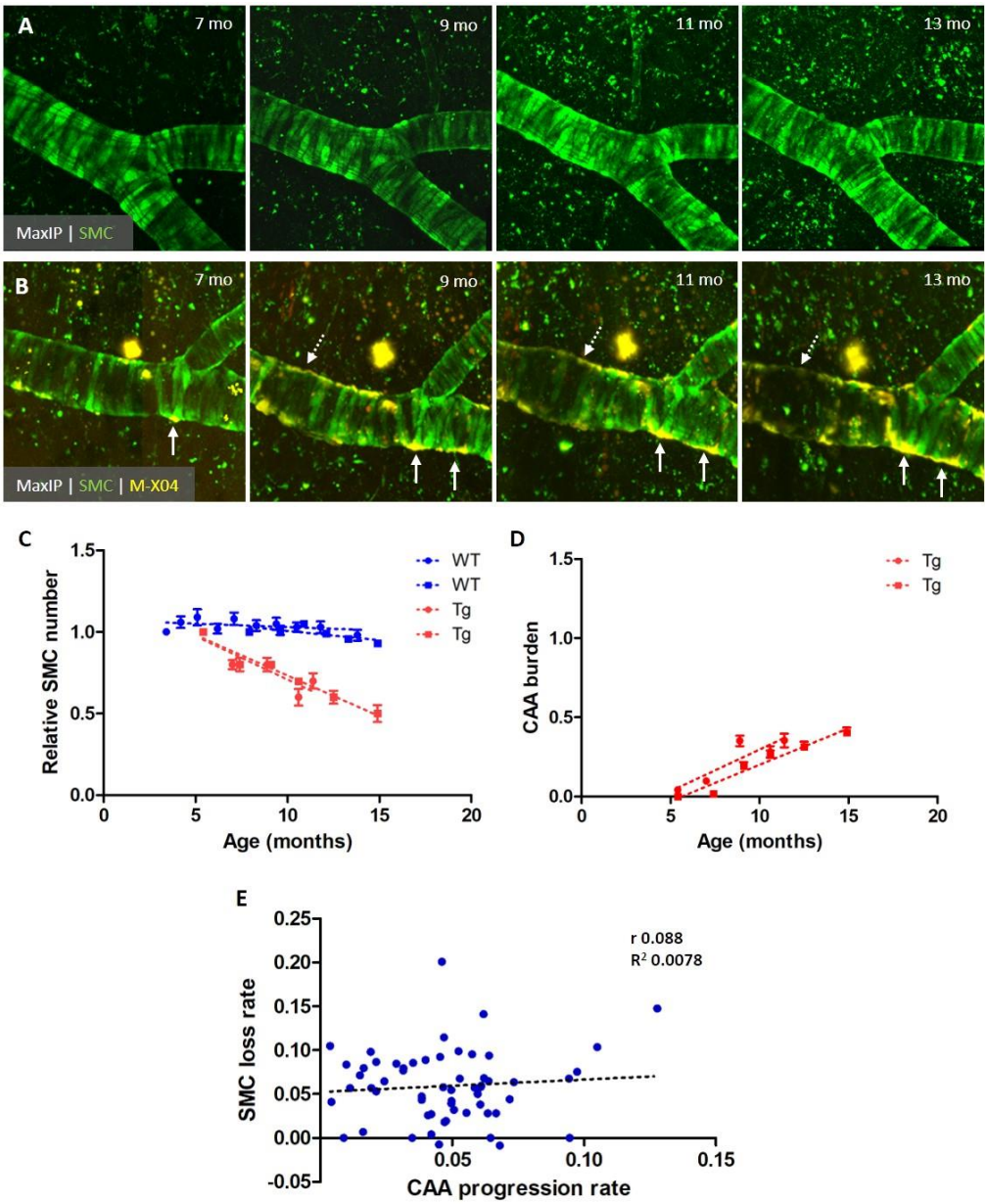

Supplemental Figure 7 (related to Figure 7). APP/PS1 mice exhibit progressive loss of vascular smooth muscle cells, independent of local cerebral amyloid angiopathy burden.

Smooth muscle cells (SMCs) were imaged monthly with *in vivo* two-photon microscopy through chronic cranial windows in APP/PS1 mice crossed with SMC/Cre/eGFP mice. No changes were observed in the appearance of SMCs over time in wild-type (WT) littermates (A). However, in transgenic (Tg) mice loss of SMCs (B, broken arrows) was observed over time in the presence of increased cerebral amyloid

angiopathy (CAA) burden (B, arrows). Note: Methoxy-X04 is depicted in yellow for better contrast with green SMCs. SMC number was quantified relative to the first imaging session for each mouse and did not change over a period of approximately 10 months in WT mice (C; mouse 1: -0.0042 ± 0.0032, n=16 ROIs, p=0.23; mouse 2: -0.011 ± 0.0058, n=23 ROIs, p=0.12). However, relative SMC number decreased over the same period in Tg mice (C; mouse 1: -0.053 ± 0.016, n=33 ROIs, p=0.043; mouse 2: -0.050 ± 0.0050, n=27 ROIs, p=0.0006). Within the Tg mice, the observed loss of SMCs was comparable with overall increase in CAA burden (D; mouse 1: 0.053 ± 0.015, n=33 ROIs, p=0.040; mouse 2: 0.046 ± 0.0054, n=29 ROIs, p=0.0011), but within each ROI at the level of individual vessel segments the rate of SMC loss was not associated with the rate of CAA progression (E; Pearson's r 0.088, p=0.50). Error bars in C and D represent standard error of the mean.